



Cite this: *CrystEngComm*, 2024, **26**, 1814

## High-pressure phase and pressure-induced phase transition of $\text{Ag}_3\text{YCl}_6$ <sup>†</sup>

Kotaro Maki,<sup>a</sup> Koki Muraoka,<sup>b</sup> Saori Kawaguchi,<sup>c</sup> Taku Tanimoto,<sup>b</sup> Akira Nakayama, <sup>b</sup> Seiya Yokokura, <sup>d</sup> Toshihiro Shimada, <sup>d</sup> Kiyoharu Tadanaga <sup>d</sup> and Akira Miura <sup>d</sup>

Received 23rd November 2023,  
Accepted 9th February 2024

DOI: 10.1039/d3ce01185b

rsc.li/crystengcomm

Hexagonal  $\text{Ag}_3\text{YCl}_6$  was found to transform into a new phase by applying pressure above  $\sim 1.5$  GPa via a diamond anvil cell. *In situ* XRD analysis revealed that the phase is monoclinic  $\text{Ag}_3\text{YCl}_6$ . The bulk modulus of the hexagonal and monoclinic phases was 37 GPa and 49 GPa, respectively. Computational investigations also supported this phase transition and bulk modulus. After releasing pressure from 2 GPa, the diffraction peaks of hexagonal  $\text{Ag}_3\text{YCl}_6$  were detected, indicating the reversibility of this phase transformation.

## Introduction

High-pressure chemistry in compressive matter is expanded by X-ray diffraction (XRD) techniques with a diamond anvil cell (DAC) and computational chemistry.<sup>1</sup> The phase transition of simple chlorides, such as  $\text{NaCl}$  and  $\text{AgCl}$ , has been studied for model systems, which transformed above 30 GPa (ref. 2) and 6.6 GPa, respectively.<sup>3</sup> Higher pressure of the  $\text{Na}-\text{Cl}$  system brings metal-rich subchlorides, such as  $\text{Na}_2\text{Cl}$  and  $\text{Na}_3\text{Cl}$ .<sup>4</sup> Moreover, the physical properties of simple chlorides under high pressure have been recently explored, such as the thermal conductivity of  $\text{NaCl}$  (ref. 5) and the ionic conductivity of  $\text{AgCl}$ .<sup>6</sup>

On the other hand, the high-pressure chemistry of ternary or more complex chlorides has yet to be explored, lacking the fundamental understanding primarily because of the experimental difficulty owing to the hygroscopic nature of chlorides. By changing the charge balance with cations with valence, complicated and defective structures afford structural variety and exciting properties.

Among ternary chlorides, alkali-metal yttrium chlorides construct rather complicated structures because of the rather large trivalent  $\text{Y}^{3+}$  (0.90 Å (ref. 7)) producing  $\text{YCl}_6$  octahedra similar to  $\text{NaCl}_6$  ones but cation vacancies and/or distortion

are essential to maintain charge balance.  $\text{Na}_3\text{YCl}_6$  presents two polymorphs at ambient pressure, namely, monoclinic and hexagonal. The hexagonal structure is a low-temperature phase with low density, while the monoclinic one is a high-temperature phase with high density.<sup>8</sup> As a result, the phase transition by increasing temperature decreases the volume.<sup>8</sup> Zirconium-doped  $\text{Na}_3\text{YCl}_6$  analogous to the monoclinic  $\text{Na}_3\text{YCl}_6$  phase has also been studied as an ionic conductor,<sup>10</sup> and  $\text{Li}_3\text{YCl}_6$  with a variety of defective rock-salt structures shows high ionic conductivity.<sup>11,12</sup>

Given the similar ionic radii of  $\text{Ag}^+$  (1.00 Å) and  $\text{Na}^+$  (0.99 Å),<sup>7</sup> it is not surprising that the known structure of  $\text{Ag}_3\text{YCl}_6$  is isostructural with the hexagonal form of  $\text{Na}_3\text{YCl}_6$ .<sup>13</sup> However, no observation has been made for  $\text{Ag}_3\text{YCl}_6$  being isostructural with the monoclinic  $\text{Na}_3\text{YCl}_6$ , which could potentially function as an  $\text{Ag}$  ion conductor, akin to the  $\text{Na}_3\text{YCl}_6$  counterpart. While it is known that heating the hexagonal  $\text{Ag}_3\text{YCl}_6$  leads to phase transformation at 350 °C, the resulting phase remains unsolved.<sup>14</sup>

In this study, we showed, for the first time, that high-pressure phase transformation converts hexagonal  $\text{Ag}_3\text{YCl}_6$  to the novel, monoclinic  $\text{Ag}_3\text{YCl}_6$  with the aid of synchrotron XRD and atomistic calculations.

## Experimental and computational methods

All operations in the experiment were performed under non-atmospheric conditions without exposure to moisture using an Ar-filled glovebox. After mixing  $\text{AgCl}$  and  $\text{YCl}_3$ , hexagonal  $\text{Ag}_3\text{YCl}_6$  was synthesized by heating at 800 °C for 3 hours, cooling to 300 °C at 250 °C h<sup>-1</sup>, and annealing at 300 °C for 10 hours.

<sup>a</sup> Graduate School of Chemical Science and Engineering, Hokkaido University, Kita 13, Nishi 8, Sapporo 060-8628, Japan

<sup>b</sup> Department of Chemical System Engineering, The University of Tokyo, Tokyo 113-8656, Japan

<sup>c</sup> Japan Synchrotron Radiation Research Institute, Sayo, Hyogo 679-5198, Japan

<sup>d</sup> Faculty of Engineering, Hokkaido University, Kita 13, Nishi 8, Sapporo 060-8628, Japan. E-mail: amirua@eng.hokudai.ac.jp

<sup>†</sup> Electronic supplementary information (ESI) available. See DOI: <https://doi.org/10.1039/d3ce01185b>



For *in situ* XRD measurement under pressure, the synthesized hexagonal  $\text{Ag}_3\text{YCl}_6$  was pressurized in a diamond anvil cell using helium gas as the pressure medium. The pressure-induced phase transition was investigated on BL10XU for the diamond anvil cell (DAC) at SPring-8 (approved numbers: 2022A1323 and 2023A1385).<sup>15</sup> The wavelength was 0.412739 Å, and the size of the X-ray beam was 6.5 micrometers vertically and 9.5 micrometers horizontally. Three pieces of rubies were installed in the DAC. The applied pressure was calculated from the average of the pressures obtained from three ruby fluorescence measurements placed in the sample chamber of the DAC. The pressure medium was He gas, and a hydrostatic pressure of approximately 0.1 to 6 GPa was applied.

For *ex situ* XRD measurement, hydrostatic pressure was applied to the synthesized  $\text{Ag}_3\text{YCl}_6$  at 2 GPa using a multi-anvil cell. The measurement was performed under ambient pressure after the release of the pressure.

We used Preferred Potential (PFP)<sup>16</sup> version 4.0.0 with D3 correction with the aid of the atomic simulation environment (ASE)<sup>17</sup> to optimize crystal structures and evaluate the bulk modulus. The initial crystal structures of hexagonal and monoclinic  $\text{Na}_3\text{YCl}_6$  were retrieved from the Inorganic Crystal Structure Database. After the isomorphic substitution of Na with Ag, structure relaxation was performed without external pressure until the maximum force became less than 0.001 eV Å<sup>-1</sup>. The optimized structures were used as inputs for structure optimization under different hydrostatic pressures until the maximum force became less than 0.02 eV Å<sup>-1</sup>. The enthalpy  $H$  was computed from the volume  $V$  and the total

energy  $E$  of the structures optimized under the pressure  $P$ , using the relation  $H = E + PV$ . Density functional theory (DFT) calculations were also conducted to assess the density of states using VASP version 6.2.1 at the optimized structures obtained by PFP. DFT calculations were performed by employing the PBE functional along with the D3 correction. A cutoff energy of 520 eV was employed. The  $k$ -point sampling was carried out using the Monkhorst–Pack method with a  $20 \times 20 \times 20$  grid.

## Results and discussion

The XRD patterns of the synthesized products showed the diffraction of hexagonal  $\text{Ag}_3\text{YCl}_6$  and residual  $\text{AgCl}$ . The lattice parameters of the synthesized hexagonal  $\text{Ag}_3\text{YCl}_6$  were determined to be  $a = 6.8822(10)$  Å and  $c = 18.338(3)$  Å, which are consistent with the previously reported values ( $a = 6.8669(14)$  Å and  $c = 18.3050(50)$  Å).<sup>14</sup>

Upon the application of hydrostatic pressure, a clear phase transition was observed around 1.5 GPa in the *in situ* XRD pattern (Fig. 1a and S1†). All the peaks except for  $\text{AgCl}$  can be assigned to the monoclinic phase, which is isostructural with monoclinic  $\text{Na}_3\text{YCl}_6$  (Fig. 1b). The intensity of the diffraction peaks did not match the simulated intensity. This can be attributed to the focused micro-sized beam that acquired only a specific position of the crystalline powder and could not obtain the information on the averaged structure.

The application of pressure has led to the broadening of the peak, as shown in Fig. 1a. This can be attributed to 1)

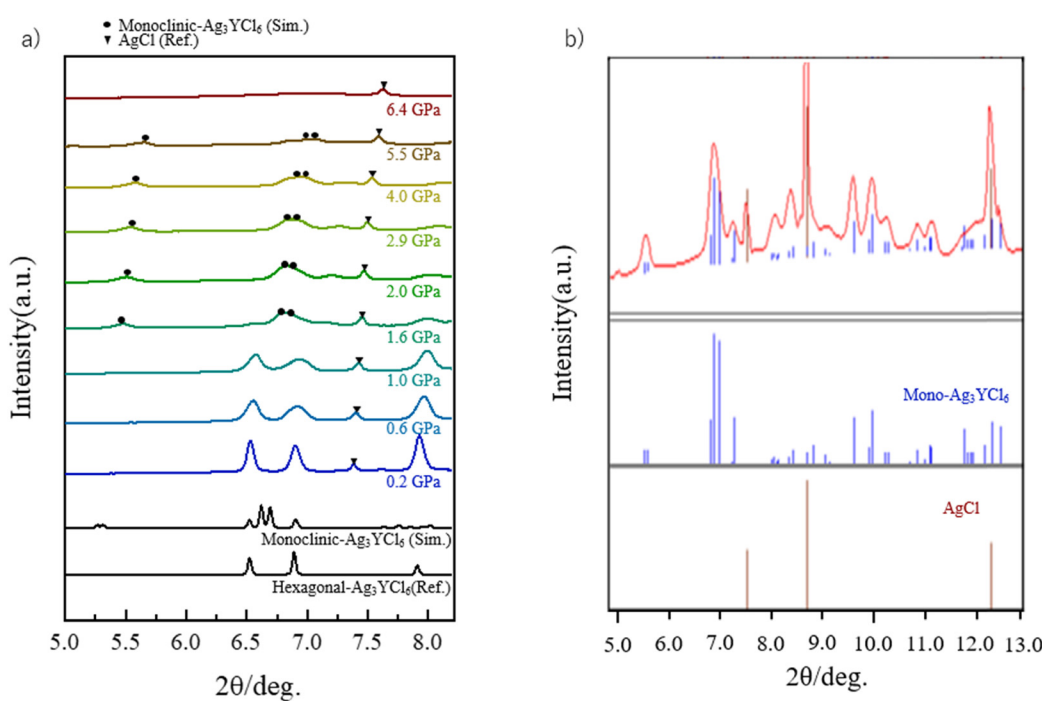


**Fig. 1** Phase transition of hexagonal  $\text{Ag}_3\text{YCl}_6$  under pressure. a) *In situ* XRD patterns of  $\text{Ag}_3\text{YCl}_6$  under hydrostatic pressure ( $\lambda = 0.412739$  Å). b) Comparison of the XRD pattern of hexagonal  $\text{Ag}_3\text{YCl}_6$  under 2.0 GPa and the simulated pattern of monoclinic  $\text{Ag}_3\text{YCl}_6$ .<sup>18</sup>



more inhomogeneous pressure detected in the differences of the Raman spectrum of ruby crystals (Table S1†), 2) lattice strain-induced broadening, and 3) lowering of the crystallite size by large volume shrinkage during the phase transformation from the hexagonal structure to the monoclinic structure. Above the pressure of 6.5 GPa, no other distinct phases are observed except for AgCl. This can be attributed to the formation of a low-crystalline or amorphous phase. While pressure-induced amorphization has been reported in various metals, oxides, and van der Waals' solids,<sup>8</sup> amorphization under high pressure in ionic compounds such as chlorides is rare. AgCl and NaCl do not undergo a phase transition into an amorphous phase at pressures below 16.1 GPa. Thus, further study is necessary to clarify this transition.

From the results of *in situ* XRD measurements, the lattice parameters at each pressure of monoclinic  $\text{Ag}_3\text{YCl}_6$  and hexagonal  $\text{Ag}_3\text{YCl}_6$  were determined (Tables S2 and S3†). Fig. 2a illustrates the pressure-dependent change in lattice volume for the monoclinic structure isostructural with  $\text{Na}_3\text{YCl}_6$  and hexagonal phases. Despite minor differences in lattice parameters, the slope of experimental data aligns with that of computational values. The experimentally determined bulk modulus was 37 GPa for hexagonal  $\text{Ag}_3\text{YCl}_6$  and 49 GPa for monoclinic  $\text{Ag}_3\text{YCl}_6$ . Meanwhile, atomistic simulations determined the bulk modulus to be 32 GPa for hexagonal  $\text{Ag}_3\text{YCl}_6$  and 49 GPa for monoclinic  $\text{Ag}_3\text{YCl}_6$ . The agreement between the experimental and simulated values implies the reliability of the bulk modulus. The lower bulk modulus of hexagonal  $\text{Ag}_3\text{YCl}_6$  can be attributed to the Ag split sites in the low-density hexagonal  $\text{Ag}_3\text{YCl}_6$ .

The phase transition of hexagonal  $\text{Ag}_3\text{YCl}_6$  was rationalized by calculating its enthalpy relative to monoclinic  $\text{Ag}_3\text{YCl}_6$  under varying pressures, using an atomistic simulation technique (Fig. 2b). At lower pressures, the hexagonal structure was more stable than the monoclinic

form, aligning with experimental observations that identify the hexagonal structure as the stable phase under ambient conditions. As the pressure increased, the enthalpy difference between the two structures decreased linearly. Fig. 2b reveals that the monoclinic structure surpasses the hexagonal structure in stability beyond a pressure of 1.29 GPa. This indicates that the theoretical phase transition pressure is 1.29 GPa, a value remarkably consistent with the experimentally determined phase transition range of 1.0–1.6 GPa (Fig. 1a).

Here, we discuss the crystal structures and phase transition. The crystal structures of the hexagonal and monoclinic phases are shown in Fig. 3. Because we could not experimentally determine the atomic position of the monoclinic cell, the proposed monoclinic structure is the calculated one (Table S4†), which is supported by the volume change shown in Fig. 2. Monoclinic  $\text{Ag}_3\text{YCl}_6$  has a cryolite-type structure, isostructural with monoclinic  $\text{Na}_3\text{YCl}_6$ . This monoclinic structure is composed of two silver (Ag) sites, three chlorine (Cl) sites, and one yttrium (Y) site. The Ag at the  $\text{Ag}_1$  site has a disordered tetrahedral shape with four coordination, while the Ag at the  $\text{Ag}_2$  site has an octahedral shape with six coordination of  $\text{AgCl}_6$ . Y also takes a six-coordinated  $\text{YCl}_6$  octahedron. By the calculation, the shortest Ag–Cl bonding in the monoclinic cells is 2.62 Å, which is shorter than that in the hexagonal cells (2.68 Å).

The occupancy of Ag is the primary difference between the crystal structures of the hexagonal and monoclinic phases. In the hexagonal structure, the Ag occupancy of  $\text{Ag}_1$  and  $\text{Ag}_2$  sites is 0.5, whereas in the monoclinic structure, the Ag occupancy of all the Ag sites is 1. Consequently, the monoclinic structure is denser, supporting the phase transition from hexagonal to monoclinic with increasing pressure.

Because  $\text{Ag}_3\text{YCl}_6$  and  $\text{Na}_3\text{YCl}_6$  are isostructures, we can expect that the phase transformation of  $\text{Ag}_3\text{YCl}_6$  is

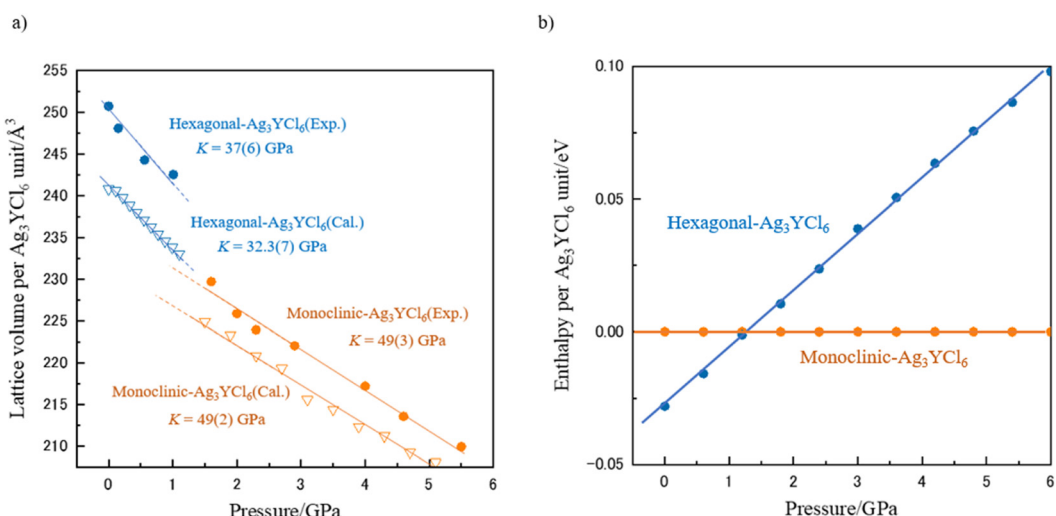
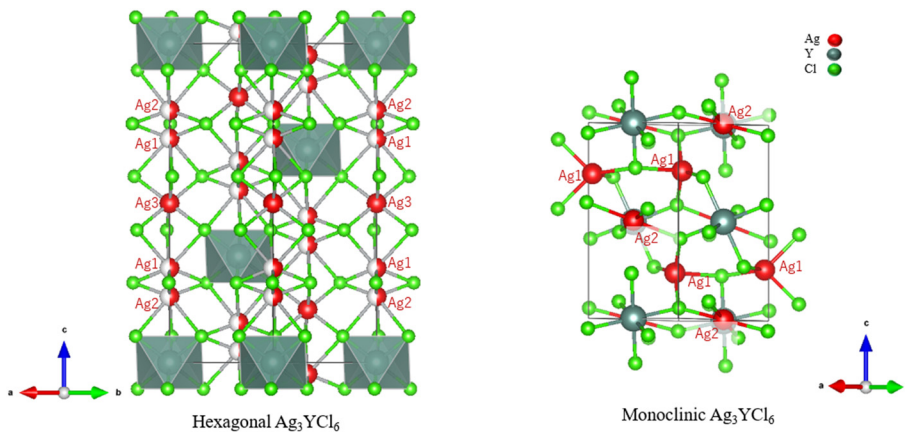


Fig. 2 a) Pressure-dependent lattice volumes of hexagonal  $\text{Ag}_3\text{YCl}_6$  and monoclinic  $\text{Ag}_3\text{YCl}_6$  (experiment: circle, simulation: triangle). b) Pressure-dependent calculated enthalpy of hexagonal  $\text{Ag}_3\text{YCl}_6$  relative to the monoclinic phase.





**Fig. 3** Crystal structure models of hexagonal and monoclinic  $\text{Ag}_3\text{YCl}_6$ . In the monoclinic phase, the Ag occupancy of  $\text{Ag}_1$  and  $\text{Ag}_2$  sites is 0.5. The crystal structure of the monoclinic phase was optimized by atomic simulation at 0 GPa and was drawn using VESTA.<sup>18</sup>

similar to that of  $\text{Na}_3\text{YCl}_6$  in a previous report.<sup>9</sup> During phase transformation, the positions of atoms at the Y and  $\text{Ag}_3$  sites in the hexagonal phase and the Y and  $\text{Ag}_2$  sites in the monoclinic phase do not change significantly.<sup>9</sup> On the other hand, the partially occupied  $\text{Ag}_1$  and  $\text{Ag}_2$  sites in the hexagonal phase are largely different from the  $\text{Ag}_1$  sites in the monoclinic phase,<sup>9</sup> indicating that the phase transition is correlated with the migration from the partially occupied positions to the fully occupied position.

This phase transformation likely resulted in changes in the electronic structure properties such as the band structures. To demonstrate this, we assessed the density of states (DOS) of hexagonal  $\text{Ag}_3\text{YCl}_6$  and monoclinic  $\text{Ag}_3\text{YCl}_6$  using DFT calculations, as depicted in Fig. S2.† The calculated band gap of 2.56 eV for the starting hexagonal  $\text{Ag}_3\text{YCl}_6$  slightly decreased to 2.51 eV for monoclinic  $\text{Ag}_3\text{YCl}_6$ . Given that the band gaps are composed of covalent Ag–Cl

bonds, the reduction in the band gap can be attributed to the shorter bonding in the monoclinic cell.

To investigate the reversibility of the phase transformation, we carried out *ex situ* XRD analysis for samples before and after pressurization of 2 GPa. As shown in Fig. 4, both samples show the patterns for hexagonal  $\text{Ag}_3\text{YCl}_6$ . Because 2 GPa is above the phase transition pressure shown in Fig. 1 and 2,  $\text{Ag}_3\text{YCl}_6$  should be transformed into the monoclinic phase, but only the hexagonal phase was observed after applying 2 GPa under ambient pressure, suggesting that the transition is reversible. The diffraction peaks of the hexagonal phase significantly broadened compared to the peaks before pressurization. This can be attributed to the crystalline strain and/or reduced crystallite size. The crystal sizes obtained before and after pressurization from the  $10\bar{2}$  peaks using Scherrer's formula were 51.9 and 26.5 nm, respectively.

## Conclusion

By using *in situ* and *ex situ* XRD with different pressures together with computational investigation, we showed that novel monoclinic  $\text{Ag}_3\text{YCl}_6$  can be obtained by pressure-induced phase transformation of monoclinic  $\text{Ag}_3\text{YCl}_6$ . The low-pressure stable phase of hexagonal  $\text{Ag}_3\text{YCl}_6$  transformed into the high-pressure stable phase of monoclinic  $\text{Ag}_3\text{YCl}_6$  above  $\sim 1.5$  GPa. The monoclinic  $\text{Ag}_3\text{YCl}_6$  phase could not be detected under atmospheric conditions, suggesting the backward transition to the hexagonal  $\text{Ag}_3\text{YCl}_6$  phase. The bulk modulus of hexagonal  $\text{Ag}_3\text{YCl}_6$  was lower than that of monoclinic  $\text{Ag}_3\text{YCl}_6$ . Further increase in pressure above 6 GPa diminished the diffraction peaks of  $\text{Ag}_3\text{YCl}_6$ .

## Conflicts of interest

There are no conflicts to declare.

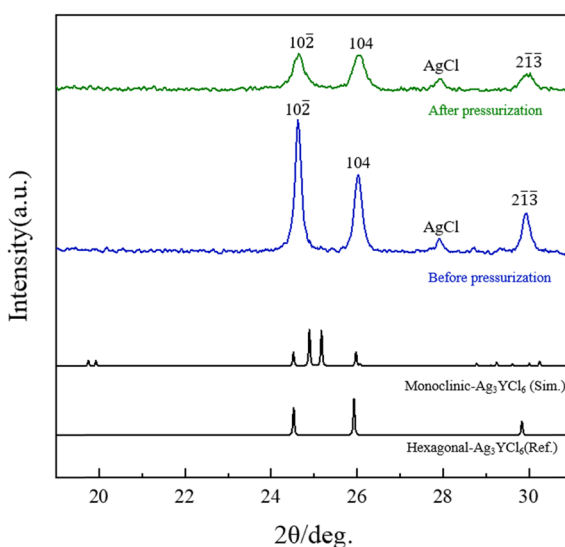


**Fig. 4** *Ex situ* XRD patterns of  $\text{Ag}_3\text{YCl}_6$  before and after pressurization using  $\text{CuK}\alpha$  radiation.

## Acknowledgements

This work was partly supported by JST SAKIGAKE JPMJPR21Q8. K. Muraoka acknowledges the support from JSPS KAKENHI (22K14751) and JST, PRESTO (JPMJPR2378).

## References

- 1 X. Dong, A. R. Oganov, A. F. Goncharov, E. Stavrou, S. Lobanov, G. Saleh, G. R. Qian, Q. Zhu, C. Gatti, V. L. Deringer, R. Dronskowski, X. F. Zhou, V. B. Prakapenka, Z. Konôpková, I. A. Popov, A. I. Boldyrev and H. T. Wang, *Nat. Chem.*, 2017, **9**, 440–445.
- 2 W. A. Bassett, T. Takahashi, H. K. Mao and J. S. Weaver, *J. Appl. Phys.*, 1968, **39**, 319–325.
- 3 S. Hull and D. A. Keen, *Phys. Rev. B: Condens. Matter Mater. Phys.*, 1999, **59**, 750–761.
- 4 W. Zhang, A. R. Oganov, A. F. Goncharov, Q. Zhu, S. E. Boulfelfel, A. O. Lyakhov, E. Stavrou, M. Somayazulu, V. B. Prakapenka and Z. Konôpková, *Science*, 2013, **342**, 1502–1505.
- 5 W.-P. Hsieh, *Sci. Rep.*, 2021, **11**, 21321.
- 6 J. Wang, G. Zhang, H. Liu, Q. Wang, W. Shen, Y. Yan, C. Liu, Y. Han and C. Gao, *Appl. Phys. Lett.*, 2017, **111**, 031907.
- 7 R. D. Shannon, *Acta Crystallogr., Sect. A: Cryst. Phys., Diff., Theor. Gen. Crystallogr.*, 1976, **32**, 751–767.
- 8 M. S. Wickleder and G. Meyer, *ZAAC*, 1995, **621**, 457–463.
- 9 F. Stenzel and G. Meyer, *ZAAC*, 1993, **619**, 652–660.
- 10 E. A. Wu, S. Banerjee, H. Tang, P. M. Richardson, J.-M. Doux, J. Qi, Z. Zhu, A. Grenier, Y. Li, E. Zhao, G. Deysher, E. Sebti, H. Nguyen, R. Stephens, G. Verbist, K. W. Chapman, R. J. Clément, A. Banerjee, Y. S. Meng and S. P. Ong, *Nat. Commun.*, 2021, **12**, 1256.
- 11 H. Ito, Y. Nakahira, N. Ishimatsu, Y. Goto, A. Yamashita, Y. Mizuguchi, C. Moriyoshi, T. Toyao, K. Shimizu, H. Oike, M. Enoki, N. C. Rosero-Navarro, A. Miura and K. Tadanaga, *Bull. Chem. Soc. Jpn.*, 2023, **11**, 1262–1268.
- 12 T. Asano, A. Sakai, S. Ouchi, M. Sakaida, A. Miyazaki and S. Hasegawa, *Adv. Mater.*, 2018, **30**, 1803075.
- 13 T. Staffel and G. Meyer, *ZAAC*, 1988, **557**, 40–44.
- 14 K. Lerch, W. Laqua and G. Meyer, *ZAAC*, 1990, **582**, 143–150.
- 15 N. Hirao, S. I. Kawaguchi, K. Hirose, K. Shimizu, E. Ohtani and Y. Ohishi, *Matter Radiat. Extremes*, 2020, **5**, 018403.
- 16 S. Takamoto, C. Shinagawa, D. Motoki, K. Nakago, W. Li, I. Kurata, T. Watanabe, Y. Yayama, H. Iriguchi, Y. Asano, T. Onodera, T. Ishii, T. Kudo, H. Ono, R. Sawada, R. Ishitani, M. Ong, T. Yamaguchi, T. Kataoka, A. Hayashi, N. Charoenphakdee and T. Ibuka, *Nat. Commun.*, 2022, **13**, 2991.
- 17 A. Hjorth Larsen, J. Jørgen Mortensen, J. Blomqvist, I. E. Castelli, R. Christensen, M. Dušak, J. Friis, M. N. Groves, B. Hammer, C. Hargus, E. D. Hermes, P. C. Jennings, P. Bjerre Jensen, J. Kermode, J. R. Kitchin, E. Leonhard Kolsbørg, J. Kubal, K. Kaasbørg, S. Lysgaard, J. Bergmann Maronsson, T. Maxson, T. Olsen, L. Pastewka, A. Peterson, C. Rostgaard, J. Schiøtz, O. Schütt, M. Strange, K. S. Thygesen, T. Vegge, L. Vilhelmsen, M. Walter, Z. Zeng and K. W. Jacobsen, *J. Phys.: Condens. Matter*, 2017, **29**, 273002.
- 18 K. Momma and F. Izumi, *J. Appl. Crystallogr.*, 2008, **41**, 653–658.

